

Numerical Simulations of Pyrolysis of Wet Charring Materials using a One-dimensional Enthalpy based model

Shivanand R. Wasan^{*1}, Pieter Rauwoens¹, Jan Vierendeels¹ & Bart Merci^{1,2}

¹. Department of Flow, Heat and Combustion mechanics (IR03), Ghent University-UGent, Sint-Pietersnieuwstraat-41, B-9000 Ghent, Belgium

². Postdoctoral Fellow of the Fund of Scientific Research – Flanders (Belgium) (FWO-Vlaanderen)

Abstract

Solid phase modelling coupled to gas phase combustion of volatiles helps to investigate the flame spread over solids. The present work focuses on the solid phase. Numerical simulations of pyrolysis of wet charring materials are performed. When the solid is exposed to an external heat flux, the model is such that the moisture present first flows out, leaving behind dry solid. This solid then further heats up and finally generates a mass flow rate of combustible volatiles during the 'pyrolysis' process, i.e. the degradation of the solid. Evaporation and pyrolysis, possibly occurring at the same time, are assumed to take place in infinitely thin fronts. Pyrolysis is thus modelled as an infinitely fast, irreversible endothermic process at the 'pyrolysis temperature' (T_{pyr}) and as such, all kinetics are ignored. The cases considered are one-dimensional in nature, in order to focus on the principal model performance. Enthalpy is the basic model variable. The temperature distribution inside the material, along with the evaporation and pyrolysis front positions, are related to the distribution of enthalpy. A piecewise linear temperature field representation is adopted.

Introduction

Flame spread is an important phenomenon in a developing fire. In order to perform numerical simulations, it is important to keep the model for the degradation of the solid phase ('pyrolysis') as simple as possible, so that calculations in the solid phase can be combined with gas phase (turbulent) combustion simulations, including radiation (and soot formation). The development of such a simple pyrolysis model is the motivation of the present work.

Depending upon the residue left after pyrolysis, there are two categories of materials, namely non-charring and charring. In non-charring solids, no residue (char) is left. The focus of our study is on charring materials, although the model is also applicable to non-charring materials. We do not discuss this in-depth here.

Many pyrolysis models have already been proposed by numerous researchers. These models vary in their complexity and domain of application, such as Arrhenius model [1]; 'integral' model [2-5]; an 'extended' integral model [6]; a moving mesh model [7]; a dual mesh model [8]. A review on pyrolysis modelling has been provided in [9]. The main objective in these models is to predict the amount of heat obtained by the solids and the time of ignition that leads to undesirable effects of fire.

The process is as follows. When the solid is heated, the temperature rises. When the temperature of the solid becomes sufficiently high, the pyrolysis process starts. Solid (virgin) material degrades and volatile combustible gases are generated. The volatile components move towards the hotter surface of the solid and ignite in the gas phase as they mix with the oxygen.

This outward motion of these volatiles becomes more difficult as the pyrolysis proceeds due to the resistance offered by the solid char matrix. This is not taken into account with the present model.

There is also inward flow of volatiles. For the moment, we ignore this inward flux.

In case of wet solids, moisture also plays a role in the global pyrolysis process, as energy is required to vaporize the water. The combination of these two processes (drying and pyrolysis) is treated in the simulations by means of an enthalpy based model.

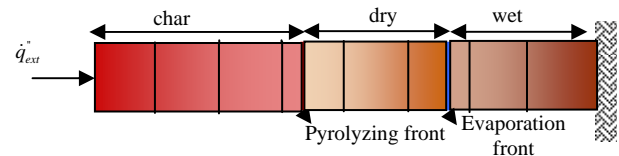


Fig. 1: One-dimensional solid under study

The solid material is thus divided into three different zones (fig.1):

- Virgin wet material
- Virgin dry material
- Char material

These different layers are distinguished by infinitely thin fronts. The wet virgin zone is separated from the dry virgin zone by an infinitely thin evaporation front maintained at evaporation temperature ' T_{evap} ', while the virgin dry zone is separated from the char zone by an infinitely thin pyrolysis front at the pyrolysis temperature ' T_{pyr} ' (fig 1). As discussed below, during a cooling phase, the front temperatures can be lower than T_{evap} and T_{pyr} .

Model description

As mentioned in the introduction, an enthalpy based model approach is adopted to simulate the pyrolysis of charring materials. We do not account for kinetics. Rather, we focus on the thermodynamic description of

¹* Corresponding author: Shivanand.Wasan@UGent.be
Proceedings of the European Combustion Meeting 2009

the phenomena. Our approach is largely based on the theoretical paper [10]. We elaborate this to obtain an enthalpy-based pyrolysis model on a fixed computational mesh. Five constituents are considered:

- (dry) virgin solid material; (v)
- char; (c)
- combustible volatiles; (g)
- liquid water ('moisture'); (w, l)
- water vapour. (w, v)

For each of the five constituents, the relation between enthalpy and temperature reads:

$$h_i(T) = h_i^o(T_{ref}) + \int_{T_{ref}}^T c_i(T) dT \quad (1)$$

The total specific enthalpy (kJ/kg) is the sum of the formation enthalpy at a reference temperature T_{ref} and the thermal enthalpy. For gases and water vapour, the thermal capacity at constant pressure is used.

The specific enthalpy at position (x) can be expressed as a mass-weighted sum of the specific enthalpies of the constituents, present at (x). Thus, the specific enthalpy at any time and any position can be written as:

$$h(x,t) = \sum_i \alpha_i(x,t) h_i(T_i(x,t)) \quad (2)$$

with $\alpha_i(x,t) = \tilde{\rho}_i(x,t) / \tilde{\rho}(x,t)$ and $\tilde{\rho}(x,t) = \sum_i \tilde{\rho}_i(x,t)$.

Here $\tilde{\rho}_i(x,t)$ denotes the local mass concentration (or 'bulk density') of this constituent. In this paper it is assumed that the specific enthalpy of each constituent is only dependent on the temperature.

In order to avoid the knowledge of formation enthalpies, the concept of 'heat of pyrolysis' is introduced. Modelling pyrolysis as an isothermal process at $T = T_{pyr}$, an amount of mass (m_v) of solid virgin material is transformed into an amount of mass (m_c) char and an amount of mass ($m_v - m_c$) pyrolysis gases, all at $T = T_{pyr}$. This endothermic process requires an amount of energy equal to $(m_v - m_c) \Delta Q_{pyr}$. For a complete elaboration, the reader is referred to [11].

The solid material is divided into 'n' fixed control volumes 'V'. These volumes are fixed throughout the simulations. The energy equation for a fixed (sub-) volume reads:

$$\frac{\partial}{\partial t} \int_V \tilde{\rho} h dV = - \int_S \vec{q} \cdot \vec{n} dS \quad (3)$$

with ' $\vec{q} \cdot \vec{n}$ ' the heat flux out of the volume 'V' through its boundary 'S'. The heat flux consists of conductive and convective terms. The convective fluxes represent enthalpy transport by the pyrolysis gases, generated at the pyrolysis front, towards the surface of the solid. We assume that the volatiles leave the solid as soon as they are generated and that they are in thermal equilibrium with the solid as they move through the char layer. Conduction is modelled by Fourier's law.

In a similar manner, the evaporation is modelled as an isothermal process at $T = 373K$. To evaporate a unit mass of liquid water an amount of energy equal to L_v is needed. L_v is the latent heat of vaporation.

Again, for a complete elaboration, the reader is referred to [11].

Solution Procedure

Figure 1 shows the basic configuration under study for wet charring materials. We recall that pyrolysis is treated as an endothermic process, taking place infinitely fast at $T = T_{pyr}$, which effectively reduces the pyrolysis region to an infinitely thin front. The flow chart in Figure 2 illustrates the solution procedure for dry charring materials. The treatment of the vaporisation front (at $T = 373K$) is similar to the treatment of the pyrolysis front. Both phenomena, pyrolysis and evaporation are treated here as an irreversible process. This implies that the fronts cannot move backwards, but the front temperature can drop below T_{pyr} or 373K. We first briefly discuss the solution procedure for dry charring materials. For more details, the reader is referred to [13].

Starting from the initial conditions, time steps $\Delta t = t^{n+1} - t^n$ are taken until the end of the simulation. From the most recent situation, the conduction and convection fluxes are computed first in each computational cell. Stepping from time t^n to t^{n+1} occurs in an iterative manner. We denote the iteration levels, for the evolution from t^n to t^{n+1} as $n+1, k$ or $n+1, k+1$, where the index k or $k+1$ indicates what values are used within this iterative procedure. From the fluxes, the enthalpy update is computed from Eq. (3).

From the new enthalpy field, the temperature field, the position of the pyrolysis front and the pyrolysis front temperature must be reconstructed. As long as no pyrolysis process is taking place, only the temperature field must be reconstructed. Here, we describe what must be done when there is a pyrolysis front.

If the pyrolysis process is ongoing, the pyrolysis front temperature is constant, equal to $T_f^{n+1, k+1} = T_f^{n+1, k} = T_{pyr}$. Thus, if $T_f^{n+1, k} = T_{pyr}$, the enthalpy update leads to a new temperature field $T_i^{n+1, k+1}$ and a movement of the pyrolysis front to a new position $x_f^{n+1, k+1}$. The front is allowed to move backwards during the iterative procedure, but it must not move back to a position $x_f^{n+1, k+1} < x_f^n$, as pyrolysis is an irreversible process. Thus, we check this. If $x_f^{n+1, k+1} \geq x_f^n$, there is no problem and we check convergence of the iterative procedure. If the convergence criterion is met, the next time level $n+1$ is achieved. If not, we go to the next iteration.

We now describe what happens if any of the above mentioned tests is 'not true'. First, it is possible that $T_f^{n+1, k} < T_{pyr}$, which means that the pyrolysis process stops (e.g. due to insufficient incoming heat flux for the pyrolysis process to continue). Then the pyrolysis front does not move and the new temperature field $T_i^{n+1, k+1}$ and pyrolysis front temperature

$T_f^{n+1,k+1}$ are computed. In the case of heating, it is possible that $T_f^{n+1,k+1} > T_{pyr}$. If this is true, we clip the front temperature to $T_f^{n+1,k+1} = T_{pyr}$ and go to the next iteration. In this next iteration, the test $T_f^{n+1,k} = T_{pyr}$ will be true and the pyrolysis front will be allowed to move. Note that, when the vapour left the char, the evaporation front is treated in the same manner as the pyrolysis front (using 373K instead of T_{pyr}).

The second test fails if $x_f^{n+1,k+1} < x_f^n$. If so, we clip the front position to $x_f^{n+1,k+1} = x_f^n$ and we must compute the front temperature (indeed, if the solution for the front position were a backward motion due to the enthalpy update, this is prohibited and cooling of the pyrolysis front is computed instead). From that point onwards, we proceed as just described.

In [13], we applied the model to a wide range of one-dimensional configurations of dry charring materials. We very briefly mention some of the results and then apply the model to wet charring material. Ambient temperature and initial temperature in the solid are set to 300K.

Influence of solid thickness

We illustrate that the model captures well the effect of the solid thickness. We use the moving grid results of [6] as numerical reference results. The thickness of the solid is varied from 2mm (thermally thin material) to 50mm (thermally thick). The boundary conditions are fixed: the front surface is exposed to a constant externally imposed heat flux of 50kW/m² and the back surface is perfectly insulated. A time step size of 0.1s was used in the simulation. The total number of fixed cells was 40.

Results and discussion

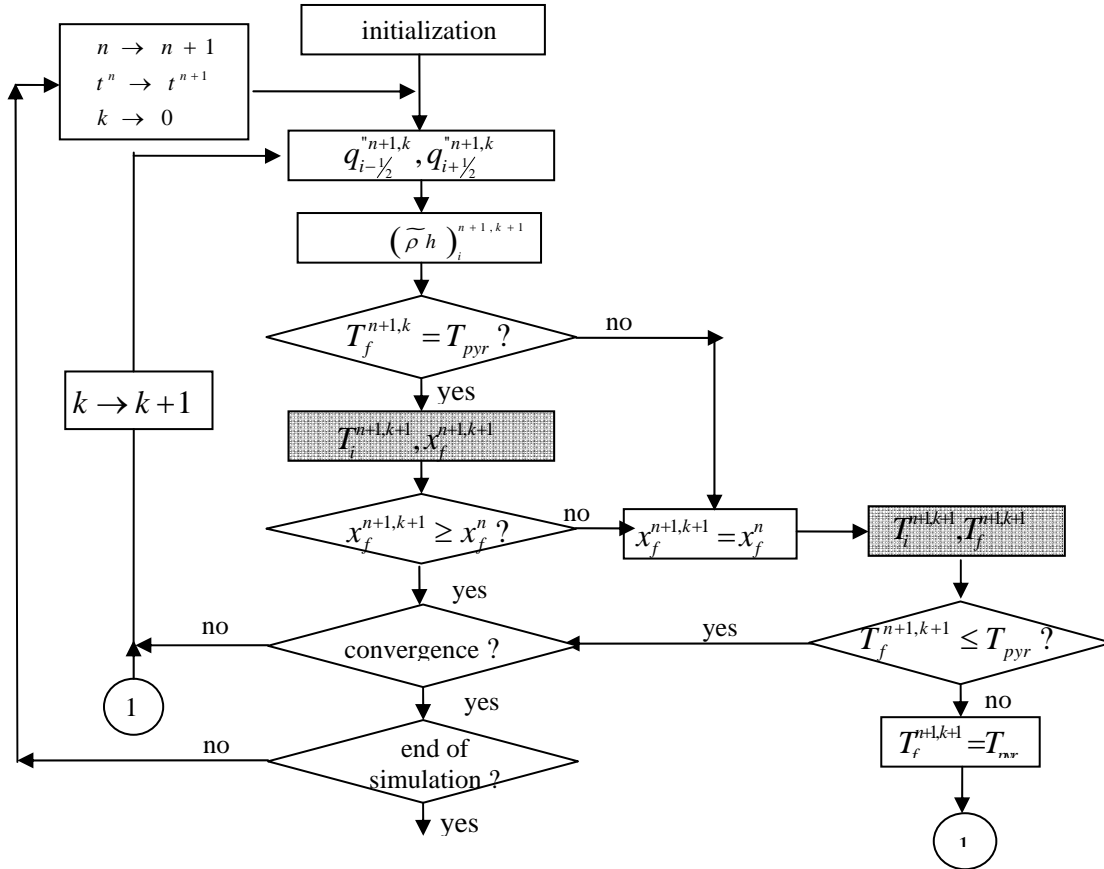


Fig. 2 Enthalpy model solution procedure

The thermo-physical properties are [6]:

$$\rho_v=600\text{kg/m}^3, \rho_c=60\text{kg/m}^3, c_v=c_c=2500\text{J/(kgK)}, k_v=0.36\text{W/(mK)}, \\ k_c=0.23\text{W/(mK)}, c_g=0\text{J/(kgK)}, \Delta Q_{pyr}=8.7 \cdot 10^5 \text{J/kg}, T_{pyr}=648\text{K}, \\ \varepsilon=1.0, h=15\text{W/m}^2\text{K}.$$

Figure 3 proves good agreement with the moving grid results over the entire range of thicknesses [6]. Pyrolysis starts earlier for the smaller thickness, due to more rapid heating of the material up to the pyrolysis temperature. For thickness larger than 10 mm, the start of pyrolysis remains practically unchanged. The heating process is then as if the solid were of infinite thickness.

For the thermally thin materials ($L < 10$ mm), a single peak is observed in the mass flow rate. The peak is higher for the smaller thicknesses (more rapid heating and faster pyrolysis front motion).

For the thermally thick materials, there are two peaks. The second peak is due to the so called ‘back effect’ [4].

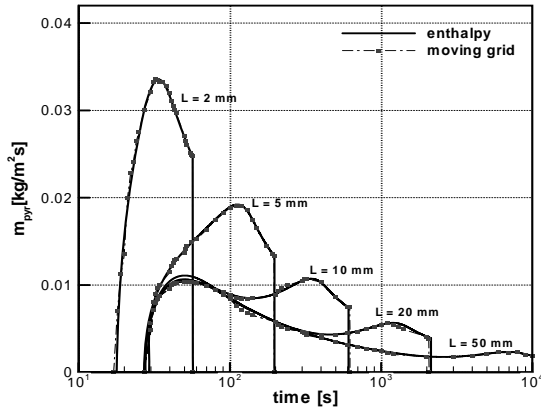


Fig. 3: Mass flow rate of pyrolysis gases (different material thicknesses).

Effect of boundary condition on the back side

As second illustration, we vary the back side boundary condition, describing the convective heat loss as follows:

$$\dot{q}_{bs}'' = h_{bs} (T_{bs} - T_{amb}) \quad (5)$$

Unless mentioned otherwise, we use the same model parameters and material properties as in the previous section. Radiative emission at the back surface is ignored, as typically the temperature T_{bs} is not high.

Figure 4 (top left) confirms the agreement with the moving grid model results again. When the pyrolysis front approaches the back boundary, the second peak (back effect) is only seen for sufficiently low values of the back boundary convective heat transfer coefficient. Indeed, there is no ‘piling up’ of heat when heat losses through the back surface are too high.

In [6], it is discussed that the integral model suffers the deficiency that mass flow rate curves cross each other when ‘ h_{bs} ’ is varied. This unphysical feature is

not observed with the present model, as illustrated in the zoom (figure 4, top right).

Figure 4 (bottom left) shows the effect of h_{bs} on the front and back surface temperatures (T_s and T_{bs}). Obviously, there is little effect on T_s . As h_{bs} increases, T_{bs} increases less and less rapidly, due to relatively higher heat losses through the back surface. Interestingly, differences become visible for $t > 250$ s, which is also the period where differences become visible in the pyrolysis gases mass flow rates (top right figure). In other words, from $t = 250$ s onwards, the back surface boundary condition affects the pyrolysis process.

The bottom right picture of fig. 4 reveals the position of the pyrolysis front as function of time. Obviously, the higher h_{bs} , the lower the pyrolysis mass flow rate and the slower x_f increases in time. Interestingly, for $h_{bs} = 20\text{W/m}^2\text{K}$, the pyrolysis process stops after a while: x_f does not increase any more for $t > 10000$ s. In other words, an equilibrium situation is met.

It is a very appealing model feature that the stopping of the pyrolysis process is automatically predicted when there is insufficient net incoming heat flux.

Wet charring materials

We now discuss simulation results for wet charring materials, using the material properties from [14]. The solid is 3cm thick. The thermo-physical properties of the material considered are:

$$\rho_v = 710 \text{ kg/m}^3, \rho_c = 180 \text{ kg/m}^3, L_v = 2.27 \cdot 10^6 \text{ J/kg}, \\ c_{vd} = 1460 \text{ J/(kgK)}, c_c = 1100 \text{ J/(kgK)}, k_{vw} = 0.31 \text{ W/(mK)}, \\ k_{vd} = 0.24 \text{ W/(mK)}, k_c = 0.10 \text{ W/(mK)}, T_{pyr} = 550 \text{ K}, \\ \Delta Q_{pyr} = 4.18 \cdot 10^5 \text{ J/kg}, h = 10 \text{ W/(m}^2\text{K)}, \varepsilon = 0.9, \\ c_g = 1900 \text{ J/(kgK)}, c_{w,v} = 2000 \text{ J/(kgK)}, c_{w,l} = 4184 \text{ J/(kgK)}$$

The indices v,w and v,d indicate wet virgin and dry virgin respectively. The time step size is 0.5s. A total of 50 cells are used in the simulations. The solid has a thickness of 3cm. The external heat flux is 40kW/m^2 .

We compare results for dry material and for a moisture content of 14%. Figure 5 shows the mass loss rate (left), the temperature at several depths (middle) and the front positions (right). The top row is for simulation up to 10000s, while the bottom row shows the simulations only up to 100s.

In the wet material, first the water starts to vaporize when the surface temperature reaches 373K. The moisture obviously leaves the solid much earlier than flammable volatiles, as, in our model, pyrolysis begins when the surface temperature reaches T_{pyr} . From then on, two fronts move and we add the mass flow rates to determine the total mass flow rate.

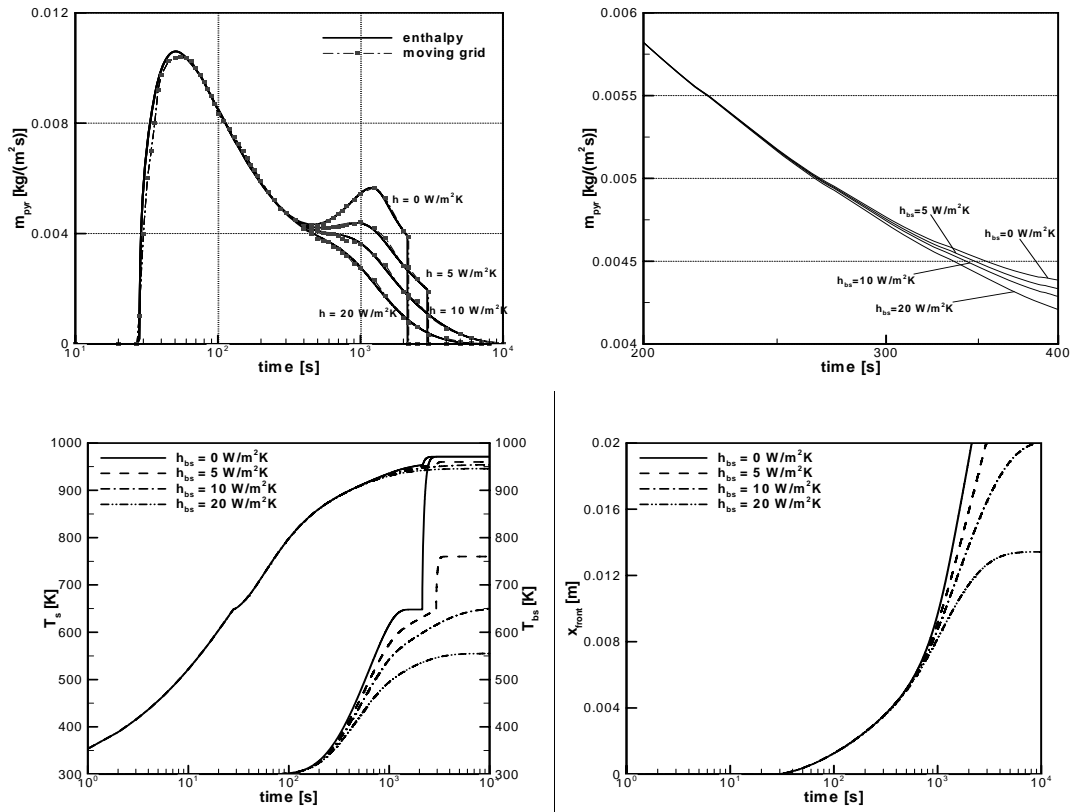


Fig. 4: Influence of back surface boundary condition (h_{bs}) and fixed front surface boundary condition ($h_s = 10\text{W/m}^2\text{K}$); mass flow rate of pyrolysis gases (top left); zoom ($t = 200\text{s} - 400\text{s}$, top right); front and back surface temperature T_s and T_{bs} (bottom left); pyrolysis front position x_f (bottom right).

The dashed line in figure 5 (left) corresponds to the mass loss rate due to moisture evaporation. Moisture evaporation starts when $T_s=373\text{K}$ (after 5s, see fig.5 bottom left). The pyrolysis process starts only when the surface temperature reaches T_{pyr} . This occurs at $t=32\text{s}$. The dash dotted-dotted line is the total amount of mass flow rate, obtained by addition of the two mentioned mass flow rates. Figure 5 shows that, for dry material (solid line), pyrolysis start earlier (after 11s) than for the wet material. This is due to the fact that evaporation consumes energy in the wet material. When the evaporation front reaches the back side of the solid, the pyrolysis mass flow rate increases (fig. 5 top left).

The temperature evolution confirms this. The rise is slower in the wet material. Obviously, it also takes longer for the temperature to rise for positions that are farther away from the front surface. The evolution of the evaporation and pyrolysis front positions reveals that the pyrolysis front moves slower than the evaporation front. It is also slower for the case of wet material than

for the dry material. The front moves faster when the evaporation front has reached the back surface.

Conclusions

We presented an enthalpy based pyrolysis model. Application of the model reveals that numerical reference results, obtained with the more complex moving grid model, are well reproduced.

Comparison of dry and wet materials reveals that pyrolysis process is slower in case of wet materials. This is due to heat, consumed to vaporize water present in the solid.

Acknowledgement

This project G.0130.06 is funded by Fund of Scientific Research - Flanders (Belgium) (FWO-Vlaanderen).

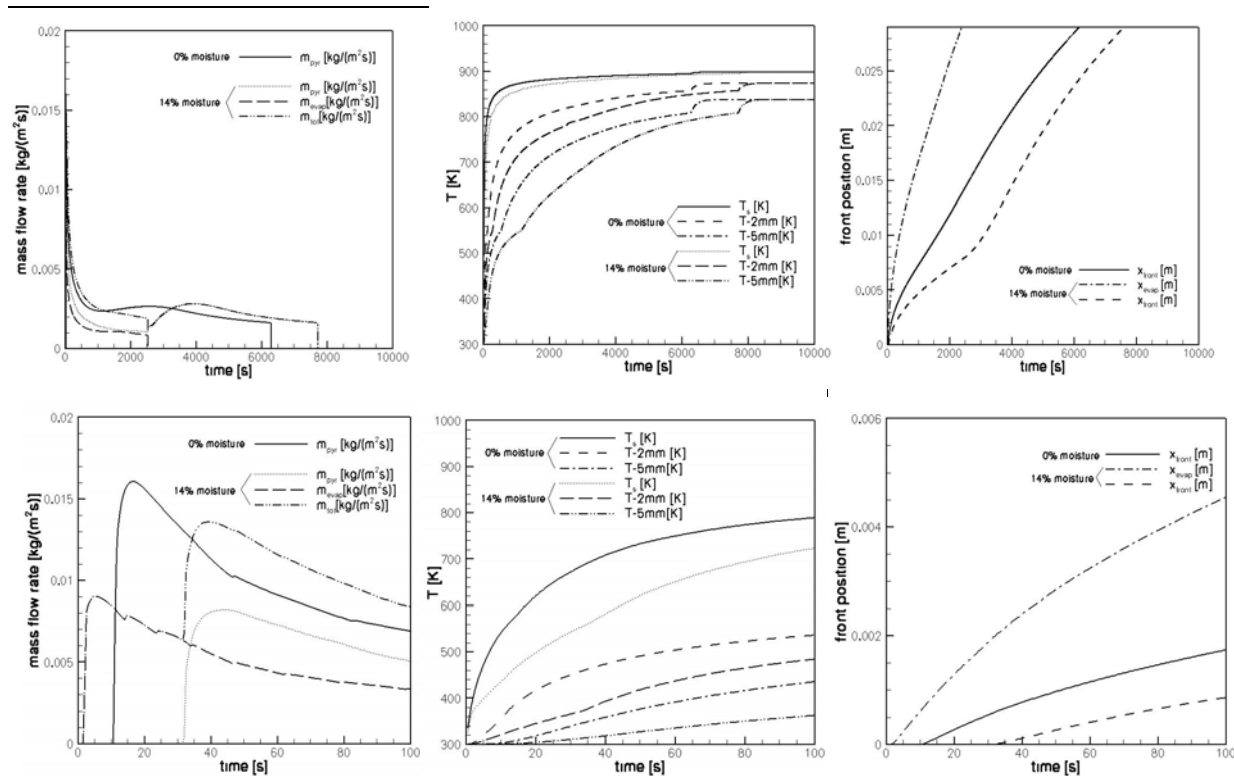


Fig. 5: Mass flow rate (left), temperature evolution at different depths (middle) and front positions (right). Top row: up to 10,000s; bottom row: up to 100s.

References

1. C. Di Blasi, Processes of Flame Spreading over the Surfaces of Charring Fuels: Effects of the Solid Thickness, *Combustion and Flame*, vol. 97, pp. 225-239, 1994.
2. B. Moghtaderi, V. Novozhilov, D. Fletcher, and J. H. Kent, An Integral Model for the Transient Pyrolysis of Solid Materials, *Fire and Materials*, vol. 21, pp. 7-16, 1997.
3. F. Jia, E. R. Galea, M. K. Patel, Numerical Simulation of the Mass Loss Process in Pyrolyzing Char Materials, *Fire and Materials*, vol. 23, pp. 71-78, 1999.
4. M. J. Spearpoint and J. G. Quintiere, Predicting the burning of wood using an integral model, *Combustion and Flame*, vol. 123, pp. 308-325, 2000.
5. W. G. Weng, and W. C. Fan, A pyrolysis model of charring materials considering the effect of ambient oxygen concentration, *Fire and Materials*, vol. 31, pp. 463-475, 2007.
6. E. Theuns, B. Merci, J. Vierendeels and P. Vandevelde, Critical evaluation of an integral model for the pyrolysis of charring materials, *Fire Safety Journal*, vol. 40, pp. 121-140, 2005.
7. E. Theuns, J. Vierendeels, P. Vandevelde, Validation of the integral model for the pyrolysis of charring materials with a moving grid, *J. of Computational and Applied Mathematics*, vol. 168, pp. 471-479, 2003.
8. Z. Yan and G. Holmstedt, CFD and Experimental Studies of Room Fire Growth on Wall Lining Materials, *Fire Safety Journal*, vol 27, 201-238, 1996.
9. Di Blasi C. Modelling and Simulation of Combustion Processes of Charring and Non-Charring Solid Fuel. *Prog. Energy Combust. Sci.* 1993. vol 19; 71-104.
10. Kung, H.C., A Mathematical Model of Wood Pyrolysis, *Combustion and Flame*, 1972, vol 18, 185-195.
11. Wasan, S. R., Rauwoens, P., Vierendeels, J., and Merci, B., An enthalpy-based pyrolysis model for charring and non-charring materials in case of fire. Part I: Model description, *Combustion and Flame* (in preparation).
12. Wasan, S. R., Rauwoens, P., Vierendeels, J., and Merci, B., An enthalpy-based pyrolysis model for charring and non-charring materials in case of fire- Part II: Application to basic test cases, *Combustion and Flame* (in preparation).
13. Wasan, S. R., Rauwoens, P., Vierendeels, J., and Merci, B., Application of an Enthalpy Based pyrolysis model in the Numerical Simulations of Pyrolysis of charring materials, *Fire and Materials* (submitted).
14. B. Benkoussas, J.-L. Consalvi, B. Porterie, N. Sardoy, J.-C. Loraud, Modelling thermal degradation of woody fuel particles, *International Journal of Thermal Sciences*, 46 (2007) 319-327.